Biosensors and Bioelectronics 107 (2018) 94–102

Contents lists available at ScienceDirect

Biosensors and Bioelectronics

journal homepage: www.elsevier.com/locate/bios

# A dye-sensitized solar cell acting as the electrical reading box of an immunosensor: Application to CEA determination

Liliana A.A.N.A. Truta, Felismina T.C. Moreira, M. Goreti F. Sales*

*BioMark, Sensor Research/ISEP, School of Engineering, Polytechnic Institute of Porto, Portugal*

ARTICLE INFO

*Keywords:*
Cancer biomarker
Immunosensor
Electrochemical Biosensor
Dye-Sensitized Solar Cell
Biological sample
Urine sample

ABSTRACT

Monitoring cancer biomarkers in biological fluids has become a key tool for disease diagnosis, which should be of easy access anywhere in the world. The possibility of reducing basic requirements in the field of electrochemical biosensing may open doors in this direction. This work proposes for this purpose an innovative electrochemical immunosensing system using a photovoltaic cell as an electrical reading box. Immunosensing ensures accuracy, the electrochemical-ground of the device ensures sensitivity and detectability, and the photovoltaic cell drives the system towards electrical autonomy. As proof-of-concept, Carcinoembryonic antigen (CEA) was used herein, a cancer biomarker of clinical relevance.

In brief, a conductive glass with a fluorine doped tin oxide film was used as conductive support and modified with anti-CEA by means of a bottom-up approach. All stages involved in the biochemical modification of the FTO surface were followed by electrochemical techniques, namely electrochemical impedance spectroscopy and cyclic voltammetry. This electrode acted as counter electrode of a dye-sensitized solar cells, and the electrical output of this cell was monitored for the different concentrations of CEA. Under optimized conditions, the device displayed a linear behaviour against CEA concentration, from 5 pg/mL to 15 ng/mL. The immunosensor was applied to the analysis of CEA in urine from healthy individual and spiked with the antigen.

Overall, the presented approach demonstrates that photovoltaic cells may be employed as an electrical reading box of electrochemical biosensors, yielding a new direction towards autonomous electrochemical biosensing.

## 1. Introduction

Biosensors are analytical devices that convert molecular recognition of a specific analyte into a measurable signal via a transducer, allowing quick responses, low cost and little requirements (Florescu et al., 2007; Sin et al., 2014; Turner, 2013). Among the different approaches in clinical analysis, electrochemical immunoassays hold a great impact in the literature (Turner, 2013). Immunoassays involve antigen/antibody reactions, inspired in the immune response (Turner, 2013; Emon, 2007). The use of antibody ensures appropriate selectivity towards a target compound, even when this compound is in very low concentrations. Electrochemical immunosensors are of special interest herein, due to their simplicity, easy miniaturization, specificity, selectivity, high sensitivity and rapid analysis (Teixeira et al., 2014). Although using an enzymatic reaction, glucose meters are a public icon of electrochemical biosensors. In general, the combination of antibodies and electrochemical biosensors has been proven successful in many applications (Turner, 2013).

This works emerges a novel biosensor technology that consists on integrating an electrochemical immunosensor inside a photovoltaic (PV) cell. PV cells generate current from light with reasonable efficiency (Wei et al., 2010) and may therefore lead electrochemical-based biosensors towards an electrical-independent approach. The first step in this direction consists in evaluating the impact of an immunosensor on the PV and understanding if the electrical performance of such new system depends on the concentration of a given target compound. To pursue this target, two key elements are identified next: the type of the PV and the target compound to be tested in this proof-of-concept design.

There are different types of PV cells. Dye-sensitized solar cells (DSSCs) have attracted much attention due to their low cost, easy manufacture and high energy conversion efficiency (Grätzel, 2001; O'Regan and Grätzel, 1991). DSSCs contain (a) a photoanode electrode, (b) a redox system electrolyte and (c) a cathode or counter electrode (CE) (Shirke et al., 2011; Hagfeldt et al., 2010). Merging a biosensor and a DSSC could be as easy as using one of these two electrodes

* Correspondence to: BioMark, Sensor Research/ISEP, School of Engineering, Polytechnic Institute of Porto, R. Dr. António Bernardino de Almeida, 431, 4200-072 Porto, Portugal.
*E-mail addresses:* goreti.sales@gmail.com, mgf@isep.ipp.pt (M.G.F. Sales).

https://doi.org/10.1016/j.bios.2018.02.011
Received 13 November 2017; Received in revised form 2 February 2018; Accepted 2 February 2018
Available online 07 February 2018

(photoanode or cathode) as the biosensor, provided that the biosensor itself would be constructed on a conductive glass support that could be interfaced within the final DSSC. Eventually, one could try to replace any of these two electrodes. From a practical perspective, the photoanode is more sensitive to water-content components, hindering its interaction with water-based samples. Replacing the CE would be simpler, if the sensing element displayed electrocatalytic properties towards the redox probe. In alternative to the typical platinum-based CEs (Hagfeldt et al., 2010), carbon-based materials may be employed. These include graphite (Yen et al., 2009), graphene (Bon et al., 2010), carbon nanotubes (Yen et al., 2009); conducting polymers (Gholamkhass and Holdcroft, 2011; Yen et al., 2009); or conductive inks (Dang et al., 2015; Yang et al., 2012) containing metal nanoparticles. The most widely used materials are silver nanoparticles, due to their simple preparation, high-yielding, low viscosity and thus easy to flow under the conductive substrate surface, low resistivity and good electrical properties (Gliga et al., 2014; Yang et al., 2012). Thus, the CE is prepared herein with a conducting carbon-silver ink, which may be interfaced with antibodies.

As proof-of-concept, Carcinoembryonic antigen (CEA) was selected herein as target compound. CEA is an important tumour marker employed in clinical diagnosis of colorectal cancer (Lech et al., 2016). Many immunoassay-based analytical approaches have been described in the literature for CEA detection (Casey and Kofinas, 2008; Hammarström, 1999; Kemmegne-Mbouguen et al., 2014; Liu et al., 2010; Lv et al., 2010; Miao et al., 2014; Shi and Ma, 2011; Tan et al., 2006; Emon, 2007), which are typically expensive, complex and time consuming, also requirying specially equipped laboratories and highly qualified personnel. Electrical-based techniques such as potentiometry (Wang et al., 2010), and amperometry (Kemmegne-Mbouguen et al., 2014; Lv et al., 2010) have also been described. Overall, all these methods would benefit from the new approach proposed herein, which is simple in terms of device set-up and expects to yield suitable analytical features, while targeting electrical independency in a near future.

Thus, this work proposes (1) a different and simple immunosensor design for CEA, employing simple chemistry strategies that allow suitable orientation of the Ab-CEA on top of the modified conductive support; and (2) merging this biosensor on a DSSC. The electrode design is optimized and the biosensor is tested in both formats: conventional modified glass and working as the CE of the DSSC. The system is further successfully calibrated in real urine samples spiked with the protein.

## 2. Experimental section

### 2.1. Reagents and solutions

All chemicals were of analytical grade and water was deionized or ultrapure Milli-Q laboratory grade. Ethanol absolute from Panreac (Spain); acetonitrile from Scharlau (Spain); acetic acid glacial (100% p.a.) and ethylene glycol (analytical reagent) from Analar Normapur (USA); phosphate buffered saline (PBS) pellets, E404, biotechnology grade, from Amresco (USA); ethylenediamine and silver nitrate ($AgNO_3$) from Merck (Germany); potassium hexacyanoferrate III ($K_3[Fe(CN)_6]$), potassium hexacyanoferrate II ($K_4[Fe(CN)_6]$) trihydrate and iodine ($I_2$) from Riedel-de-Häen; bovine serum albumin (BSA), CEA from human fluids (CEA); *cis*-bis(isothiocyanato)bis(2,2´-bipyridyl)−4,4´-dicarboxilate) ruthenium(II) (dye N3), *N*-ethyl-*N*′-(3-dimethylaminopropyl)carbodiimidehydrochloride (EDAC), 1-hexyl-3-methylimidazolium iodide (HMII), *N*-hydroxysuccinimide (NHS), lithium iodide, monoclonal anti-carcinoembryonic antigen antibody produced in mouse (Ab-CEA), 4-tert-butylpyridine (TBP) and titanium (IV) oxide ($TiO_2$) (> 99.7%, anatase, < 25 nm) from Sigma-Aldrich (USA). The Ab-CEA solution was used after a 10 × dilution of the commercial product in PBS buffer (pH 7.4), and was used throughout this work.

### 2.2. Equipment

The electrochemical measurements were made in a potentiostat/galvanostat, Autolab PGSTAT302N, from Methrom (United Kingdom), equipped with a Frequency Response Analysis (FRA) module, interfaced to computer and controlled by NOVA 1.9 software. DSSC measurements were made in the same equipment, coupled to a LED driver accessory, also from Methrom (United Kingdom). Electrochemical impedance analysis (EIS) was performed in a frequency range 0.01–10,000 Hz. The photocurrent density-photovoltage (J-V) response of the solar cell was obtained using PV measurement system, under 77.7 mW/cm$^2$, having a LED driver operating with 450 mA output warm white LED. The cell area was fixed at 3.6 cm$^2$. Sintering was made in a Nabertherm GmbH P330 oven (Germany).

Solid materials were characterized by Fourier Transform Infrared Spectrometry (FTIR), using a Nicolet iS10 FTIR spectrometer, from Thermo Scientific (USA), couple to the Attenuated Total Reflectance (ATR) sampling accessory of diamond contact crystal, also from Nicolet. The spectra were collected under room temperature/humidity control, after background correction. The number of scans for sample and background was set to 100. The *x*-axis ranged from 650 to 4000 cm$^{-1}$ and *y*-axis expressed in % transmittance. The resolution was 4000.

Solid materials were also analyzed by Raman spectrometry, using a DXR Raman spectroscope from Thermo Scientific (USA), equipped with a confocal microscope. The Raman spectra was collected with a 532 nm excitation laser, in the Raman shift from 200 to 3500 cm$^{-1}$, for 0.3 mW power and exposures of 90 s, in combination with a 50 × objective magnification for focus and collection of Raman-scattered light. The confocal aperture was set to 25 μm pinhole.

### 2.3. FTO electrode modification

A fluoride-doped tin oxide (FTO, sheet resistance 13.0 Ω/sq) glass was obtained from Sigma-Aldrich (USA), and was cut into 2.0 × 1.5 cm size slices. The slices were ultrasonically cleaned, first for 15 min in acetone and after for 15 min in deionized water, and then dried in nitrogen atmosphere.

The cleaned FTO electrodes were modified with an organic silver conductive ink (OSC ink). For the synthesis of the OSC ink, silver nitrate (0.08 g/mL) was first dissolved completely with a reducing agent (1.11 g/mL, ethyleneglycol), under vigorous stirring, at room temperature. Then, a complexing agent (0.90 g/mL, ethylenediamine) was added dropwise, to the previous solution, over a few min. (~ 60 s), followed by 500 μL of deionised water (Chang et al., 2012; Dang et al., 2015; Tao et al., 2013; Yang et al., 2012). The chemical reaction occurred slowly, changing from the pale yellow to a dark brown solution, revealing the formation of silver particles (Dang et al., 2015). The synthesized OSC ink was deposited on the surface of the pre-treated FTO coated glass and thermally sintered, set to a temperature of 200 °C, along 10 h. Thus, a silver film formed onto the FTO layer (FTO/Ag-$NH_2$) and acted as support of the immunosensing layer.

### 2.4. Assembly of the immunosensing layer

The immunosensor (FTO/Ag-$NH_2$/Ab-CEA) was assembled as represented in Fig. 1A. A solution of ethylenediamine (30 mg/mL) was placed first on the previous silver film for 2 h, at room temperature. Different conditions were tested to improve the efficiency of amine binding, in terms of time (during 30 min, and 1 and 2 h) and temperature (4, 25 and 60 °C).

In parallel, a solution of Ab-CEA was activated to bind the amine support. This was done by reacting the Ab-CEA solution with NHS (50 mg/mL) and EDAC (10 mg/mL), prepared in PBS buffer (pH 7.4), for 10 and 15 min, respectively. Next, the activated Ab-CEA was added to the Ag-$NH_2$ layer, at 4 °C, for 1 h. The resulting surface was then loaded with BSA solution (33.2 mg/mL), for 2 h, at 4 °C, in order to

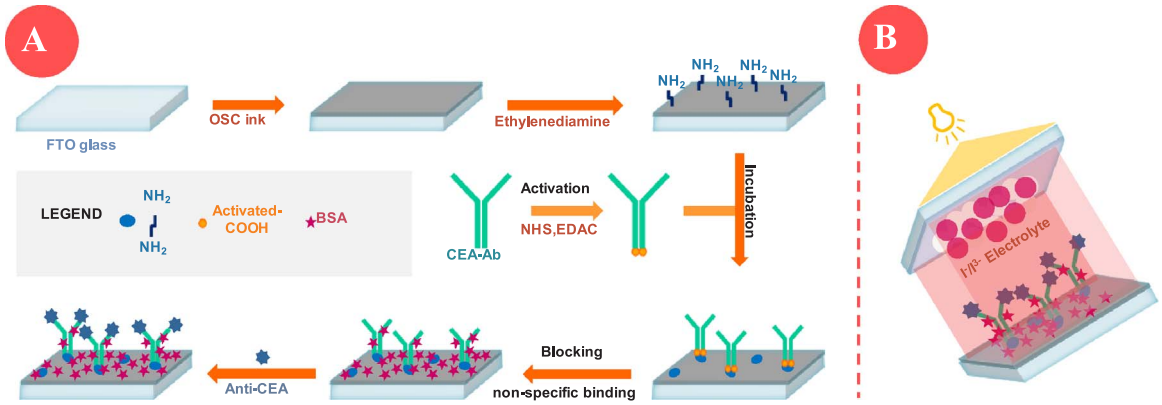


**Fig. 1.** Schematic design of the immunosensor for CEA detection (A) and its application in a DSSC (B).

block the non-specific binding areas of the antibody.

The antigen binding was made by incubating 25 µL of a CEA solution of increasing concentrations, for 30 min, to allow the affinity reaction between the Ab-CEA and CEA. The working CEA solutions were prepared in PBS buffer (pH 7.4) by accurate dilution of a stock solution of 25 µg/mL, and had varying concentrations: 1–25 ng/mL, 0.01–25 ng/mL and 0.005–15 ng/mL. CEA was also detected in real urine samples doped with this antigen, ranging from 1.0 to 25 ng/mL and 0.0050–15 ng/mL. After each incubation, the surface was washed with PBS prior to redox probe (iron or iodide based) measurements by EIS and cyclic voltammetry (CV), for all CEA concentration ranges tested.

### 2.4.1. Electrochemical biosensing

Electrochemical measurements were made in an electrochemical cell at room temperature by using CV and EIS assays, which were conducted with a redox probe of 5.0 mM $[Fe(CN)_6]^{3-/4-}$ (1:1) mixture solution or 10 mM $I_2$ and 20 mM LiI mixture, both prepared in PBS buffer, pH 7.4. The immunosensor response to CEA concentration levels was tested by EIS at an open circuit potential (OCP), using a sinusoidal potential perturbation with amplitude of 0.01 V and a number of frequencies equal to 100, logarithmically distributed over a frequency range of 0.01 − 10,000 Hz. EIS data were fitted to a Randles equivalent circuit using the implemented NOVA software from Autolab. In CV measurements, the potential was scanned from − 1.0 to + 1.0 V, at a sweep 50 mV/s, for 10 cycles.

Measurements of the conventional set-up of the biosensor were performed in a conventional three-electrode system assembly, consisting of a silver chloride reference electrode (Ag/AgCl//0.6 mol/Kg KCl), a carbon CE and the immunosensor FTO/Ag-$NH_2$/Ab-CEA.

## 2.5. DSSC assembly and performance

A typical DSSC contains (a) a photoanode electrode, (b) a cathode, and (c) a redox system electrolyte (Shirke et al., 2011; Hagfeldt et al., 2010). Each element is described next.

### 2.5.1. Preparation of the electrodes

The (a) photoanode combines (i) a transparent conductive material, which allows light to pass through; (ii) a mesoporous oxide layer (typically $TiO_2$) deposited on the conductive transparent layer to activate electronic conduction; (iii) and a monolayer of dye (usually ruthenium complexes) at the surface of the mesoporous oxide layer to enhance light adsorption. Herein, the photoanode consisted of a $TiO_2$ paste, prepared by dispersing 6.0 g of $TiO_2$ anatase nanopowder in 8.0 mL of ethanol, 1.0 mL of acetic acid and in 1.0 mL of ultrapure water. This mixture was stirred for 1 h, at room temperature and the resulting paste was printed on the FTO coated glass by using the doctor blade method. Next, the photoanodes were annealed at 450 °C for 1 h (Dembele et al., 2013; Mehmood et al., 2014), cooled down to 80 °C and finally immersed in a dye bath solution, at room temperature, in the dark (Mehmood et al., 2014). This dye solution was composed by an ethanolic solution of dye N3 (0.5 mM). The photoanode electrode was removed after 24 h from the dye solution, washed with ethanol and dried.

The (b) cathode or CE consisted of an FTO conductive glass sheet, coated with a catalyst, catalysing the redox couple regeneration and the electron collection from the external circuit (Gong et al., 2012; Mehmood et al., 2014; Wu et al., 2015). Herein, the CE was made as described in Section 2.4.

### 2.5.2. Set-up of the DSSCs

The PV cells were assembled with the photoanode (FTO/$TiO_2$ paste/dye) and the cathode (immunosensor, FTO/Ag-$NH_2$/Ab-CEA). These electrodes were separated by a redox system consisting of an electrolyte (normally an organic solvent containing a redox mediator, such as $I^-/I^{3-}$ couple, iodide/triiodide), which is in contact with the dye and restores it during operation.

Herein, two different electrolyte solutions were employed: (1) an electrolyte solution commonly used in DSSCs, containing 5.0 mM $I_2$, 100 mM LiI, 600 mM HMII and 500 mM TBP in acetonitrile; (2) and another electrolyte containing 10 mM $I_2$ and 20 mM LiI in PBS buffer (called herein as the *new electrolyte*). Each electrolyte was casted between the electrodes (photoanode and cathode). The schematic representation is shown in Fig. 1B, corresponding to a cell area of 3.6 $cm^2$.

### 2.5.3. Electrochemical measurements of the DSSCs

DSSC measurements were evaluated by EIS analysis, performed with the FRA module in a frequency range 0.01–10,000 Hz, and by J-V response, using a LED driver operating under 450 mA output warm white LED, with 77.7 mW/$cm^2$. This is a 2-electrode set-up system.

## 3. Results and discussion

### 3.1. Preparation of the immunosensor support

The schematic representation of the stepwise functionalization process to assemble the immunosensor is shown in Fig. 1A. The first stage consisted on cleaning and controlling the FTO glass support. The next stage consisted on the modification of the conductive glass support (FTO glass) with a layer of silver-based ink, aiming to cast silver nanoparticles on the FTO. Silver nanoparticles hold electrocatalytic features against the iodide probe, ensuring a suitable performance of the DSSC.

Before binding the Ab-CEA, the FTO/Ag surface was modified with amine groups. The antibodies had been first casted directly on this silver support, but binding to the antigen was not effective and the electrochemical signals offered little reproducibility. This modification consisted in the addition of ethylenediamine to the silver-based material, allowing a reaction between silver and the amine groups in

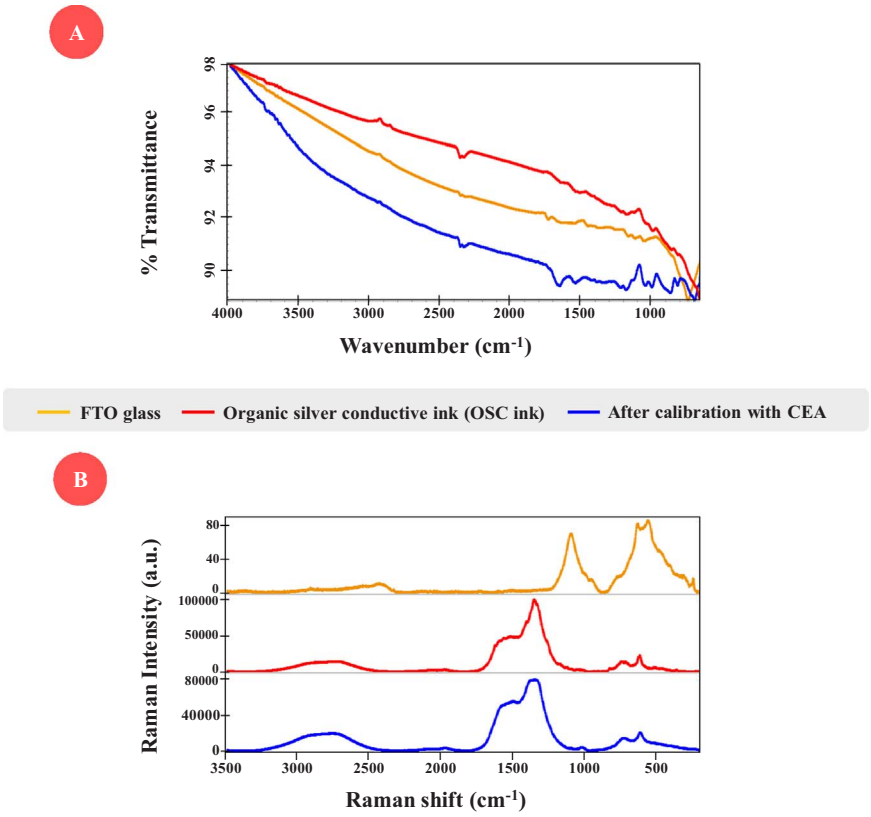


**Fig. 2.** Characterization of several layers casted on glass by **(A)** FTIR and **(B)** Raman spectrometry.

ethylenediamine. The resulting layer was identified as FTO/Ag-$NH_2$. Overall, amine groups are capable of interacting with proteins while preventing significant conformation changes. The presence of such conductive ink was evidenced by naked eye and was followed by FTIR and Raman spectra, compared to the non-modified FTO-glass.

The FTIR spectra are shown in Fig. 2A. The spectrum of FTO glass showed broad bands due to the vibrational modes of the Sn-O-Sn oxide lattice, below 800 $cm^{-1}$. These Sn − O − Sn groups were evidenced, abundantly, at ~800 $cm^{-1}$. This band was shifted to lower wavenumbers in the FTO glass modified with OSC ink (Scipioni et al., 2014). The FTIR spectrum of the OSC ink film also revealed a weak band around 2950 and 2850 $cm^{-1}$, assigned to the presence of asymmetric and symmetric C − H stretching. The broad peak around 1575 $cm^{-1}$ and the weak band between 1000 and 1100 $cm^{-1}$ were assigned, respectively, to the C − N and C − O stretching vibrations. The presence of a peak around 692 $cm^{-1}$ may correspond to the O − C − C in plane bending vibration, which means that the ethylenediamine was coordinated to silver nitrate, in which an electron of the amino group was donated to the silver atom, thus decreasing the electron density of the amino group and resulting in a weaker NH group peak (Yang et al., 2012).

The Raman spectra of the same materials are shown in Fig. 2B. The spectrum of bare FTO glass evidenced a broad band between 400 and 900 $cm^{-1}$. This region evidenced two small peaks, at 563 and 628 $cm^{-1}$ that could be assigned to Sn − O and Sn − O − Sn stretching vibrations, respectively (Kumar et al., 2011; Truta and Sales, 2015). The band at 1088 $cm^{-1}$ could be assigned to the asymmetric Si − O − Si stretching vibration and the ionic character of the Si − O group (Socrates, 2004; Truta and Sales, 2015). This band at 1088 $cm^{-1}$ could also be related to the doping of tin oxide glass with fluorine, compound that has a strong band at 1100 − 1000 $cm^{-1}$, due to the C − F stretching vibration (Gong et al., 2012). The silver-based carbon ink on the FTO shifted the bands assigned to Sn − O and Sn − O − Sn stretching vibrations to higher Raman shift values (to 618 and 742 $cm^{-1}$, respectively). The presence of carbon in the ink was revealed by two intense bands, at 1350 $cm^{-1}$ and 1540 $cm^{-1}$, related to the $-CH_2$ deformation vibration and to the C=C vibration (Socrates, 2004; Truta and Sales, 2015). Around 2500 − 3100 $cm^{-1}$, this spectrum showed a broad band, which could be associated to the stretching vibration of C − H bond in the N − C − H group (Socrates, 2004; Truta and Sales, 2015).

The changes in the electrical features out coming from the presence of the ink were also followed by EIS. The corresponding Nyquist plots are shown in Fig. 3. In these plots, the resistances to charge transfer ($R_{ct}$) corresponded to the diameter of each semicircle observed. Accordingly, the FTO-glass (Fig. 3A) was the material of higher $R_{ct}$ (~667 kΩ), followed by FTO-glass modified with the OSC ink, with an $R_{ct}$ of ~1806 Ω (Fig. 3B). The presence of the amine groups (Fig. 3C) also enhanced significantly the base level of resistance (up to ~8073 Ω).

### 3.2. Binding the antibody to the support

Antibodies may bind to a given support in numerous ways, among which different chemistries may be employed. Herein, a simple approach developed by us in the past was used, consisting of a simple activation of the –COOH groups within the Ab-CEA (Ferreira and Sales, 2014). The activation of this group allows a mild reaction with the amine groups on the FTO support to form amide products, and contributes to a suitable orientation of the antibody on the support. As the Fc terminal of an antibody is composed by –COOH groups, it is expected that the antibody binds to the FTO/Ag-$NH_2$ support through this point, thereby allowing that both paratope sites remain free for subsequent antigen binding (Wu et al., 2015).

The –COOH groups of the Ab-CEA were activated via a carbodiimide reaction by EDAC/NHS. In this, the –COOH group formed a highly reactive *O*-acylisourea intermediate that reacted rapidly with NHS, to produce a succinimide ester intermediate (Truta and Sales, 2015). This intermediate is expected to react with the free amine groups on the

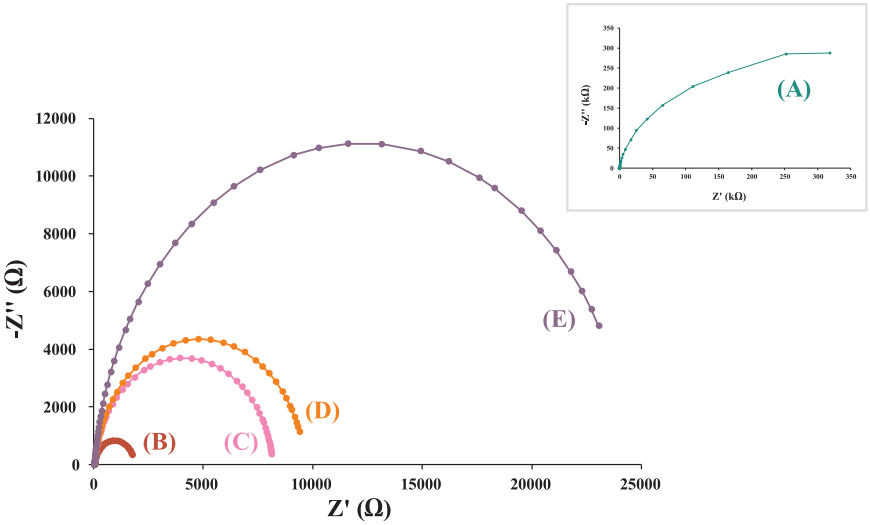


**Fig. 3.** EIS spectra obtained on the assembly of the immunosensor through an iodide redox probe, including (A) bare FTO electrode; (B) FTO/Ag: modification of FTO support with an OSC ink layer; (C) FTO/Ag-$NH_2$: addition of amine groups on top of the conductive layer with ethylenediamine; (D) FTO/Ag-$NH_2$/Ab-CEA: binding of the antibody to the amine surface, and (E) FTO/Ag-$NH_2$/Ab-CEA/BSA: blocking of non-specific binding sites with BSA.

FTO/Ag-$NH_2$, yielding a covalent binding of the antibody on this surface. This reaction is favoured under mild conditions and no significant conformation changes are expected to occur in the antibodies.

The incubation of the activated Ab-CEA on the FTO/Ag-$NH_2$ is expected to bind the antibodies to the platform, in a covalent way and with a suitable orientation. The resulting material is the immunosensor FTO/Ag-$NH_2$/Ab-CEA. The EIS data collected with FTO/Ag-$NH_2$/Ab-CEA supports confirmed the presence of Ab-CEA in the immunosensor. In general, antibodies are huge proteins with non-conductive features that hinder the electrical signals passing through the materials. Thus, the electrical effect yields an increase in the observed $R_{ct}$ up to ~9600 Ω (Fig. 3D), when compared to the FTO/Ag-$NH_2$ (Fig. 3C).

Following the typical immunoassays, the last final stage of the immunosensor assembly consisted in blocking free peptide region on the support that could otherwise allow unspecific binding. For this purpose, the FTO/Ag-$NH_2$/Ab-CEA support was incubated in a high amount of BSA, a simple and low-cost protein commonly used as blocking of the non-specific sites in immunosensors. The resulting FTO/Ag-$NH_2$/Ab-CEA(-BSA) support (Fig. 3E) yielded the most significant increase in the $R_{ct}$ value observed throughout the assembly of the immunosensor (up to ~24.5 kΩ) and confirmed the presence of bound BSA.

### 3.3. Optimization of CEA binding

CEA is a glycoprotein (Pinho and Reis, 2015) involved in cell adhesion, directly linked to different cancer conditions besides colorectal cancer, such as breast, ovarian, lung, gastric, pancreatic, liver, and medullary thyroid cancers (Stowell et al., 2015). CEA levels may be detected in different biological samples, as serum, blood and urine, playing therefore an important role in the pre-diagnosis evaluation and in the follow-up examination during therapy. The normal levels of CEA biomarker in healthy adults is about 3.0–5.0 ng/mL, and higher levels of this biomarker can signal the presence of cancer (Hammarström, 1999).

The binding of CEA into the FTO/Ag-$NH_2$/Ab-CEA(-BSA) support was made by incubating the protein for a fixed time, washing with buffer and reading the response of the same support under a standard redox probe. A change in the $R_{ct}$ yielded by this probe was directly linked to changes in the electrical properties of the surface. In general, the presence of bound CEA on the surface was detected by an $R_{ct}$ increase. This feature was used to optimize the response of the immunosensor against different conditions.

The first study consisted in understanding how changing the temperature and time of incubation of ethylenediamine could improve the linkage of the activated Ab-CEA to silver-based carbon ink film. For this purpose, the incubation of amine groups was evaluated at different temperatures (4, 25 and 60 °C), along different times (30 min, 1 h and 2 h), for each temperature described, and against an iron redox probe. EIS assays (Fig. S1) demonstrated that when the CEA immunosensor did not contain ethylenediamine, the $R_{ct}$ increased by the addition of Ab-CEA but the blocking effect of the BSA was negligible, which was not consistent with the presence of the antibody on the surface. In addition, the repeatability of this procedure was poor, suggesting that the antibody binding was not stable, due to the week interactions established with the carbon/silver material. The subsequent tests included always ethylenediamine. From all variables tested, only the 25 °C incubation for 2 h was able to produce consistent results. Overall, the other conditions indicated that the temperature (lower or higher than 25 °C) affected the behaviour of the FTO/Ag surface alone, thereby changing all subsequent data. Thus, the condition that ensured a good linkage between Ab-CEA and the silver film formed onto the FTO layer was the incubation at 25 °C for 2 h.

The impact of the CEA binding on the surface was also followed by FTIR and Raman spectroscopy. The FITR spectra after incubating CEA of high concentration is shown in Fig. 2. The major transmittance peak is centred at 1680 $cm^{-1}$, which represents C=O stretching vibrations, arriving from the several functional groups containing this bond. Also, other major peaks at 1516, 1179 and 1039 $cm^{-1}$ were identified and assigned to the C−N stretching vibrations (secondary amides), N−H bending (tertiary amides) and C−O vibrations in carbohydrate moieties (Bahn and Pappelis, 2001; Lewis et al., 2013). Regarding Raman spectra, the most representative peaks are similar to those of the ink film, but their Raman shift changed: around 613 $cm^{-1}$ (− 0.10 a.u.); 716 $cm^{-1}$ (+ 0.22 a.u.); 1345 $cm^{-1}$ (− 0.20 a.u.); 1564 $cm^{-1}$ (+ 0.13 a.u.) and, around 2500–3100 $cm^{-1}$ (+ 0.35 a.u.).

### 3.4. Electrochemical performance of the immunosensor in a 3-electrode system

The analytical features of the biosensor were obtained by calibrating the system for increasing concentrations of CEA. This was done first by having PBS buffer as background of the calibrating solution and after in diluted blank urine. This study was complemented by checking the effect of having an iron or iodide-based redox probe. EIS and CV data was obtained for CEA concentrations ranging 0.005 − 15 ng/mL.

The typical data obtained with standard solutions prepared in PBS buffer and iron redox probe is shown in Fig. 4A. Overall, the Nyquits plots evidenced linear behaviour for $1/\Delta R_{ct}$ (which $\Delta R_{ct} = R_{ct(sample)}/R_{ct(blank)}$) against log(concentration) from 0.005 ng/mL up to 15 ng/mL CEA in buffer. The anionic slope was − 0.17 Ω/decade concentration

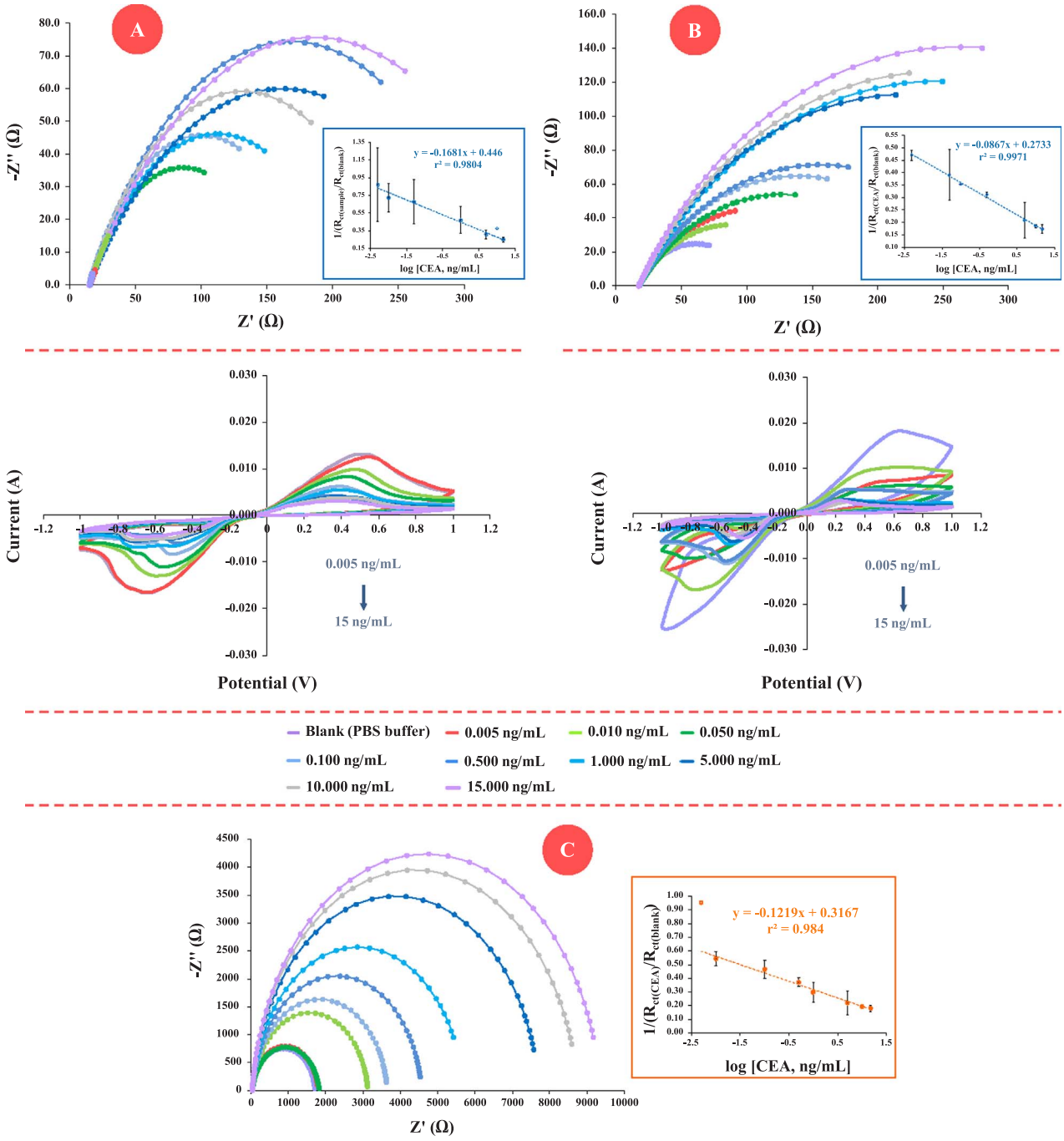


**Fig. 4.** Typical EIS data of the CEA immunosensor behaviour with different ranges of CEA concentrations, in (A) PBS solution or (B) spiked blank urine (diluted 10 × ) using an iron redox probe or (C) spiked blank urine (diluted 10 ×) using an iodide redox probe. The CV data related to the same conditions in (A) and (B) is shown below.

and the squared correlation coefficient > 0.98. The CV data was consistent with these results, also showing linear behaviour in the range of 0.005–15.0 ng/mL, with a slope − 0.15 A/decade concentration and squared correlation coefficient > 0.99, under PBS buffer solution and iron redox probe conditions (inset of Fig. 4A).

For calibrating in conditions close to urine samples, blank urine was collected from healthy volunteer and diluted 10 ×. Then, standard solutions were prepared in this diluted urine and the typical Nyquist plots obtained shown in Fig. 4B, in which an iron redox probe was used to follow-up the changes in the electrical properties. Under this condition, the linear response of the immunosensor was within the same concentration range as in buffer, having an anionic slope of − 0.087 and a squared correlation coefficient > 0.99; the linear behaviour was observed down to 0.005 ng/mL. The response under CV measurements was also consistent with the previous data, showing the same linear range, for an anionic slope of − 0.18 and squared correlation coefficient of > 0.99.

Considering that the DSSC operates with an iodide redox probe, the analytical features of the immunosensor were also evaluated against this redox probe. This was done for the same concentration range tested before and the iodide redox solution was prepared in PBS. The EIS data was collected at the OCP of this probe. Overall, the EIS calibration was linear from 0.010 ng/mL, with a slope of − 0.12 Ω/decade concentration, an LOD of 0.010 ng/mL and a squared correlation coefficient of ~0.99 (Fig. 4C). Moreover, repeated calibrations indicated that the response was precise, with standard deviations below than 10%.

Overall, these results showed a similar behaviour of the immunosensor, when evaluated by EIS assays in the same CEA concentration range against an iron redox probe or an iodide redox probe. This meant that the electrical features of FTO/Ag-$NH_2$/Ab-CEA(-BSA) remained concentration dependent, when in the presence of iodide. Therefore, this suggested that the immunosensor could be employed as the CE of the DSSC.

### 3.5. Electrochemical performance of the immunosensor as counter electrode of the DSSC

As previously explained, a DSSC was employed as the electrical reading box of the biosensor by using the FTO/Ag-$NH_2$/Ab-CEA(-BSA) as the CE within the PV cell set-up. To evaluate the potential of the analytical application of this novel approach, the device was calibrated against CEA increasing concentrations, prepared in real urine, diluted in buffer. The levels of CEA spiked into this urine blank solution ranged from 0.25 to 183.50 ng/mL and the electrochemical behaviour was evaluated by EIS and *J-V* measurements, having a redox electrolyte that was PBS- or acetonitrile-based. In general, the interfacial charge transfer process within the fabricated DSSC was first fitted into an appropriate equivalent circuit (Fig. 5), obtained by the NOVA software, and the analytical data collected under illumination.

The set-up and calibration of the device in PBS-based electrolyte are shown in Fig. 5A-B. In general, the electrochemical relative features of the assembly of this new set-up (Fig. 5A) were consistent with the previous data of the immunosensor outside the DSSC. The calibration obtained by the Nyquist plots (Fig. 5B), also confirmed a linear increase of $\Delta R_{ct}$ ($\Delta R_{ct} = R_{ct(sample)}/R_{ct(blank)}$) against the increasing of the logarithm CEA concentration. Linear behaviour was observed down to 0.25 ng/mL, with typical cationic slopes of 0.34 per decade concentration and squared correlation coefficients > 0.99 (inset in Fig. 5B). Linear responses were observed within a higher concentration range than with the immunosensor conventional set-up, but this range was within the CEA levels of clinical interest.

The evaluation of the set-up and calibration of the device in acetonitrile-based electrolyte is shown in Fig. 5C-D. As previously, the electrochemical relative features of the assembly of this new set-up (Fig. 5C) were consistent with the previous data of the immunosensor outside the DSSC, apart from the elimination of diffusion-limited process (no W element, and the Randle's circuit applied herein). The Nyquist plots (Fig. 5D) gave rise to a linear increase of $\Delta R_{ct}$ ($\Delta R_{ct} = R_{ct(sample)}/R_{ct(blank)}$) against the increasing of the logarithm CEA concentration down to 0.50 ng/mL, with typical cationic slopes of 0.69 per decade concentration and squared correlation coefficients > 0.96 (inset in Fig. 5D).

Overall, the immunosensor response inside a DSSC was concentration dependent. The linear CEA concentration range with the acetonitrile-based electrolyte was narrower than with the PBS-based electrolyte. This was a reasonable result, as proteins tend to denature in acetonitrile medium, limiting the response of the biosensor. This is especially evident for higher concentration levels, in which the antibodies and protein suffer from a cumulative effect of consecutive incubations.

### 3.6. Photovoltaic data of the immunosensor/DSSC set-up

Besides the Nyquist plots, it was possible to extract data related to the usual characterization of PV cells and to understand the impact of the immunosensor upon these cells. For this purpose, *J-V* curves were

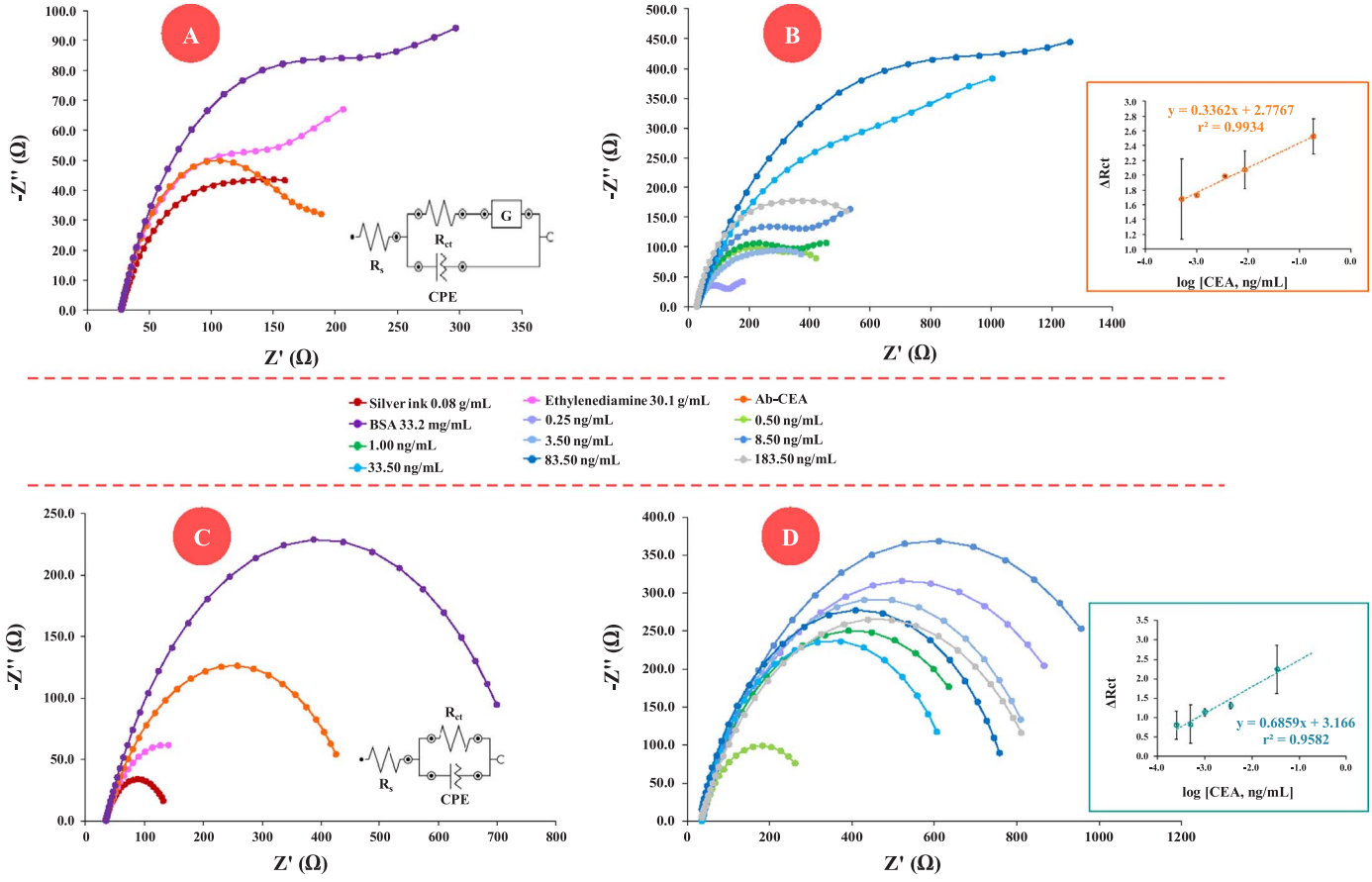


**Fig. 5.** EIS measurements of the assembly of the immunosensor designed and the corresponding calibration curves in real urine samples spiked with different CEA standard concentrations (0.25–183.50 ng/mL) obtained in a DSSC set-up. The measurements were made in the presence of different electrolytes: (A) and (B) were obtained with new electrolyte and (C) and (D) with the conventional electrolyte used for the DSSCs evaluation.

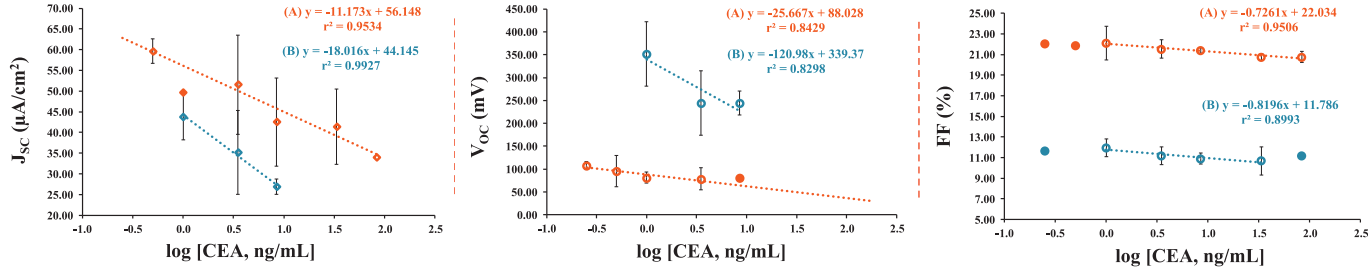


**Fig. 6.** Representative calibration curves of $J_{sc}$, $V_{oc}$ and FF of the modified DSSCs evaluated for (A) new electrolyte and (B) conventional electrolyte with the increase of the CEA concentration levels. The DSSC performance was evaluated under 77.7 mW/cm$^2$ (LED driver was operating with 450 mA output warm white LED). $J_{sc}$: Short-circuit current density; $V_{oc}$: Open-circuit voltage; FF: fill factor. Area of the cell electrode was 3.6 cm$^2$.

recorded for each stage of the set-up of the immunosensor, followed by its subsequent calibration in diluted urine. The results obtained are summarized in Table S1, displaying the values of the short-circuit current density ($J_{sc}$), the open-circuit voltage ($V_{oc}$) and the fill factor (FF).

The FF of the PV cell with FTO/Ag as cathode was of similar amplitude in both cells, containing different electrolytes. The PBS-based electrolyte displayed a ~21% FF, while the acetonitrile-based electrolyte had an FF value of ~25%. However, the subsequent modifications of the immunosensor until the CE FTO/Ag-$NH_2$/Ab-CEA(-BSA) was ready, contributed to significant variations in this value, ending in 22% when the new electrolyte was used and in ~12% when in the presence of conventional electrolyte. Thus, the overall impact of the antibodies on the CE of the cell was contained by using a PBS-based electrolyte.

The calibration procedure of the immunosensor using the PV cell as an electrical reading box was the same as in Section 3.5. It started by incubating the sensor in 0.25 ng/mL for the same period of time as in the previous studies, washing this surface and setting-up the PV cell with this material as CE; this procedure was repeated for increasing concentrations, and the resulting electrical output of the cell is listed in Table S1. These values were also plotted in Fig. 6. In general, the overall tendency of $J_{sc}$, $V_{oc}$ and FF was to decrease for increasing concentrations of CEA, thereby presenting anionic slopes. This behaviour was supported by the blocking effect of the protein upon the conductivity features of the CE. In terms of concentration dependency, the variable $J_{sc}$ seemed to be the most reliable one among the photovoltaic properties. $J_{sc}$ decreased with the increasing CEA concentrations and attained a maximum value of 59.65 μA/cm$^2$, in the new electrolyte assays, and 43.80 μA/cm$^2$ in the conventional electrolyte.

Overall, it seemed clear that the response of $J_{sc}$ seemed to be dominated by concentration and that the new electrolyte displayed wider tendencies for a linear range than the conventional acetonitrile-based electrolyte. The quality of the linear range could be improved, because there are many other new variables that need to be controlled under this new set-up, e.g., whether to recover the photoanode or to use a new electrode for each concentration reading. Still, the anionic response of the immunosensor obtained in the DSSC assays along the calibration in biological samples was similar to the response obtained in the calibration curves in spiked blank urine samples, evaluated against an iodide redox probe.

## 4. Conclusions and future perspectives

Overall, our new platform describes the disruptive integration of biosensors inside PV, trying to employ these as the electrical reading box of a biosensor. In detail, an immunosensor for CEA prepared on FTO glass displayed suitable features, when integrated inside a DSSC and after being evaluated by conventional EIS and CV electrochemical techniques. The resulting biosensor was sensitive for CEA, considering that it displayed linear responses within the concentration range of clinical interest, and it was selective for CEA in diluted urine samples, used as background medium in the preparation of standard solutions. Moreover, the CEA-immunosensor revealed a stable response, with standard deviations below 3% when evaluated in the DSSC configuration.

The future perspectives for this disruptive approach are marvellous. This apparently strange interaction between PV cells and biosensors may lead to the production of self-sustained biosensors, because a PV cell is itself an electrical energy generator. Thus, no electrical power, nor battery, may turn out necessary to have this biosensor working in the field.

As its performance is concentration dependent, its electrical output may be translated into a concentration value. Eventually, this concept may be extended to any other biomolecules and to many other bior-ecognition elements besides antibodies. Moreover, once the system is calibrated in a blank sample, it is highly likely that it will operate well in the analysis of real samples.

Further studies are currently ongoing to make the device completely self-sustained, not only regarding electrical source, but also in terms of reading box. As the PV cell provides an electrical output, this output may be also translated by numerous ways, avoiding the need for complex or portable potentiostat devices. This work is currently undergoing in BioMark sensor research.

## Acknowledgements

The authors acknowledge the financial support of European Research Council though the Starting Grant, 3P's Starting Grant/ERC (GA 311086).

## Appendix A. Supporting information

Supplementary data associated with this article can be found in the online version at http://dx.doi.org/10.1016/j.bios.2018.02.011.

## References

Bahn, P.R., Pappelis, A., 2001. IR Spectra Protein, Therm. Protein, Therm. glycoprotein 73–74.

Bon, S.B., Valentini, L., Kenny, J.M., Peponi, L., Verdejo, R., Lopez-Manchado, M.A., 2010. Electrodeposition of transparent and conducting graphene/carbon nanotube thin films. Phys. Status Solidi a-Appl. Mater. Sci. 207, 2461–2466. http://dx.doi.org/10.1002/pssa.201026138.

Casey, B.J., Kofinas, P., 2008. Selective binding of carcinoembryonic antigen using imprinted polymeric hydrogels. J. Biomed. Mater. Res. - Part A 87A, 359. http://dx.doi.org/10.1002/jbm.a.31757.

Chang, Y., Wang, D., Tai, Y., Yang, Z., 2012. Preparation, characterization and reaction mechanism of a novel silver-organic conductive ink. J. Mater. Chem. 22, 25296–25301. http://dx.doi.org/10.1039/c2jm34569b.

Dang, M.C., Dung Dang, T.M., Fribourg-Blanc, E., 2015. Silver nanoparticles ink synthesis for conductive patterns fabrication using inkjet printing technology. Advances in Natural. Sci.: Nanosci. Nanotechnol. 6. http://dx.doi.org/10.1088/2043-6262/6/1/015003.

Dembele, K.T., Nechache, R., Nikolova, L., Vomiero, A., Santato, C., Licoccia, S., Rosei, F., 2013. Effect of multi-walled carbon nanotubes on the stability of dye sensitized solar cells. J. Power Sources 233, 93–97. http://dx.doi.org/10.1016/j.jpowsour.2013.01.075.

Emon, J.M.V., 2007. Immunoassay and other bioanalytical techniques. CRC press, Taylor and Francis Group.
Ferreira, N.S., Sales, M.G., 2014. Disposable immunosensor using a simple method for oriented antibody immobilization for label-free real-time detection of an oxidative stress biomarker implicated in cancer diseases. Biosens. Bioelectron. 53, 193–199. http://dx.doi.org/10.1016/j.bios.2013.09.056.
Florescu, M., Barsan, M., Pauliukaite, R., Brett, C.M.A., 2007. Development and application of oxysilane sol–gel electrochemical glucose biosensors based on cobalt hexacyanoferrate modified carbon film electrodes. Electroanalysis 19, 220–226. http://dx.doi.org/10.1002/elan.200603714.
Gholamkhass, B., Holdcroft, S., 2011. Enhancing the durability of polymer solar cells using gold nano-dots. Sol. Energy Mater. Sol. Cells 95, 3106–3113. http://dx.doi.org/10.1016/j.solmat.2011.06.043.
Gliga, A.R., Skoglund, S., Wallinder, I.O., Fadeel, B., Karlsson, H.L., 2014. Size-dependent cytotoxicity of silver nanoparticles in human lung cells: the role of cellular uptake, agglomeration and Ag release. Particle and Fibre. Toxicology 11, 1–17. http://dx.doi.org/10.1186/1743-8977-11-11.
Gong, J., Liang, J., Sumathy, K., 2012. Review on dye-sensitized solar cells (DSSCs): Fundamental concepts and novel materials. Renew. Sustain. Energy Rev. 16, 5848–5860. http://dx.doi.org/10.1016/j.rser.2012.04.044.
Grätzel, M., 2001. Photoelectrochemical cells. Nature 414, 338–344.
Hagfeldt, A., Boschloo, G., Sun, L., Kloo, L., Pettersson, H., 2010. Dye-Sensitized Solar Cells. Chem. Rev. 110, 6595–6663.
Hammarström, S., 1999. The carcinoembryonic antigen (CEA) family: structures, suggested functions and expression in normal and malignant tissues. Semin. Cancer Biol. 9, 67–81. http://dx.doi.org/10.1006/scbi.1998.0119.
Kemmegne-Mbouguen, J.C., Ngameni, E., Baker, P.G., Waryo, T.T., Kgarebe, B., Iwuoha, E.I., 2014. Carcinoembryonic antigen immunosensor developed with organoclay nanogold composite film. Int. J. Electrochem. Sci. 9, 478–492.
Kumar, V., Govind, A., Nagarajan, R., 2011. Optical and photocatalytic properties of heavily F-doped SnO2 nanocrystals by a novel single-source precursor approach. Inorg. Chem. 50, 5637–5645. http://dx.doi.org/10.1021/ic2003436.
Lech, G., Słotwiński, R., Słodkowski, M., Krasnodębski, I.W., 2016. Colorectal cancer tumour markers and biomarkers: recent therapeutic advances. World J. Gastroenterol. 22, 1745–1755.
Lewis, S.P., Lewis, A.T., Lewis, P.D., 2013. Prediction of glycoprotein secondary structure using ATR-FTIR. Vib. Spectrosc. 69, 21–29. http://dx.doi.org/10.1016/j.vibspec.2013.09.001.
Liu, M., Jia, C., Jin, Q., Lou, X., Yao, S., Xiang, J., Zhao, J., 2010. Novel colorimetric enzyme immunoassay for the detection of carcinoembryonic antigen. Talanta 81, 1625–1629. http://dx.doi.org/10.1016/j.talanta.2010.03.014.
Lv, P., Min, L., Yuan, R., Chai, Y., Chen, S., 2010. A novel immunosensor for carcinoembryonic antigen based on poly(diallyldimethylammonium chloride) protected prussian blue nanoparticles and double-layer nanometer-sized gold particles. Microchim. Acta 171, 297–304. http://dx.doi.org/10.1007/s00604-010-0435-9.
Mehmood, U., Rahman, S., Harrabi, K., Hussein, I., Reddy, B.V., 2014. Recent advances in dye sensitized solar cells. Adv. Mater. Sci. Eng. 1–12. http://dx.doi.org/10.1155/2014/974782.
Miao, X., Zou, S., Zhang, H., Ling, L., 2014. Highly sensitive carcinoembryonic antigen detection using Ag@Au core-shell nanoparticles and dynamic light scattering. Sens. Actuators, B: Chem. 191, 396–400. http://dx.doi.org/10.1016/j.snb.2013.10.016.
O'Regan, B., Grätzel, M., 1991. A low-cost high efficiency solar cell based on dye-sensitized colloidal Tio2 films. Nature 353, 737–740.
Pinho, S.S., Reis, C., 2015. Glycosylation in cancer: mechanisms and clinical implications. Nat. Rev. Cancer 15, 540–555.
Scipioni, R., Gazzoli, D., Teocoli, F., Palumbo, O., Paolone, A., Ibris, N., Brutti, S., Navarra, M.A., 2014. Preparation and characterization of nanocomposite polymer membranes containing functionalized SnO2 additives. Membranes 4, 123–142. http://dx.doi.org/10.3390/membranes4010123.
Shi, W., Ma, Z., 2011. A novel label-free amperometric immunosensor for carcinoembryonic antigen based on redox membrane. Biosens. Bioelectron. 26, 3068–3071. http://dx.doi.org/10.1016/j.bios.2010.11.048.
Shirke, B.S., Korake, P.V., Hankare, P.P., Bamane, S.R., Garadkar, K.M., 2011. Synthesis and characterization of pure anatase TiO 2 nanoparticles. J. Mater. Sci.-Mater. Electron. 22, 821–824. http://dx.doi.org/10.1007/s10854-010-0218-4.
Sin, M.L.Y., Mach, K.E., Wong, P.K., Liao, J.C., 2014. Advances and challenges in biosensor-based diagnosis of infectious diseases. Expert Rev. Mol. Diagn. 14, 225–244. http://dx.doi.org/10.1586/14737159.2014.888313.Advances.
Socrates, G., 2004. Infrared and Raman characteristic group frequencies. Infrared Raman Charact. Group Freq. http://dx.doi.org/10.1002/jrs.1238.
Stowell, S.R., Ju, T., Cummings, R.D., 2015. Protein glycosylation in cancer. Annu. Rev. Pathol. 10, 473–510.
Tan, F., Yan, F., Ju, H., 2006. A designer ormosil gel for preparation of sensitive immunosensor for carcinoembryonic antigen based on simple direct electron transfer. Electrochem. Commun. 8, 1835–1839. http://dx.doi.org/10.1016/j.elecom.2006.08.026.
Tao, Y., Tao, Y., Wang, B., Wang, L., Tai, Y., 2013. A facile approach to a silver conductive ink with high performance for macroelectronics. Nanoscale Res. Lett. 8, 1–6.
Teixeira, S., Conlan, R.S., Guy, O.J., Sales, M.G.F., 2014. Label-free human chorionic gonadotropin detection at picogram levels using oriented antibodies bound to graphene screen-printed electrodes. J. Mater. Chem. B 2, 1852–1865. http://dx.doi.org/10.1039/c3tb21235a.
Turner, A.P.F., 2013. Biosensors: sense and sensibility. Chem. Soc. Rev. 42, 3184–3196.
Truta, L.A., Sales, M.G., 2015. Sol-gel chemistry in biosensing devices of electrical transduction: application to CEA cancer biomarker. Curr. Top. Med. Chem. 15.
Wang, Y., Zhang, Z., Jain, V., Yi, J., Mueller, S., Sokolov, J., Liu, Z., Levon, K., Rigas, B., Rafailovich, M.H., 2010. Potentiometric sensors based on surface molecular imprinting: detection of cancer biomarkers and viruses. Sens. Actuators B: Chem. 146, 381–387. http://dx.doi.org/10.1016/j.snb.2010.02.032.
Wei, D., Andrew, P., Ryhanen, T., 2010. Electrochemical photovoltaic cells—review of recent developments. J. Chem. Technol. Biotechnol. 85, 1547–1552.
Wu, J., Lan, Z., Lin, J., Huang, M., Huang, Y., Fan, L., Luo, G., 2015. Electrolytes in dye-sensitized solar cells. Chem. Rev. 115, 2136–2173. http://dx.doi.org/10.1021/cr400675m.
Yang, W., Liu, C., Zhang, Z., Liu, Y., Nie, S., 2012. One step synthesis of uniform organic silver ink drawing directly on paper substrates. J. Mater. Chem. 22, 23012–23016. http://dx.doi.org/10.1039/c2jm34264b.
Yen, M., Yen, C., Liao, S., Hsiao, M., Weng, C., Lin, Y., Ma, C.M., Tsai, M., Su, A., Ho, K., Liu, P., 2009. A novel carbon-based nanocomposite plate as a counter electrode for dye-sensitized solar cells. Compos. Sci. Technol. 69, 2193–2197. http://dx.doi.org/10.1016/j.compscitech.2009.06.003.